Impact of nonlinear radiative nanoparticles on an unsteady flow of a Williamson fluid towards a permeable convectively-heated shrinking sheet

Abstract

Purpose- The impact of nanoparticles on an unsteady flow of a Williamson fluid past a permeable convectively heated shrinking sheet is examined numerically.

Design/methodology/approach – In sort of the solution of the governing differential equations, suitable transformation variables are used to get the system of ODEs. The converted equations are then numerically solved via the shooting technique.

Findings – The impacts of such parameters on the velocity profile, temperature distribution and the concentration of nanoparticles are examined through graphs and tables. The results point out that multiple solutions are achieved for certain values of the suction parameter and for decelerating flow $(A \le 0)$, while for accelerating flow $(A > 0)$ the solution is unique. Further, the non-Newtonian parameter reduces the fluid velocity and boosts the temperature distribution and concentration of nanoparticles in the first solution, whilst the reverse drift is noticed in the second solution.

Originality/value – We think that the current results are new and significant which are utilized in many applications such as biomedicine, industrial, electronics and solar energy. The results have not been considered elsewhere.

Keywords: Unsteady flow; nanofluid; Williamson fluid; nonlinear radiation; convective boundary condition.

1. Introduction

There are several fluids of engineering and industrial significance such as multigrade oils, blood polymers, petroleum production, composite material, fruit juices and shampoos that

display the viscoelastic behavior. These fluids cannot be described by a simple model of Newtonian fluids. Due to diversity of flow in nature, different non-Newtonian models have been recommended by researchers. Amongst several models, there is one important non-Newtonian model which is the Williamson fluid model. The Williamson fluid model has a definite advantage over other non-Newtonian fluid models in the sense that it contains both minimum viscosity and maximum viscosity which gives better results for pseudoplastic fluids (apparent viscosity at infinity does not tend to zero). Williamson (1927) proposed this model which describe the equations of viscous flow of the pseudo-plastic fluids and verified the results experimentally. Nadeem et al. (2013) developed the two-dimensional flow equations of Williamson fluid towards a stretched surface and obtained the series solution using homotopy analysis method. Khan and Khan (2014) obtained the series solution of four types of steady flow of Williamson liquid. The two-dimensional steady flow of a Williamson fluid past a stretched sheet filled with nanoparticles was inspected by Nadeem and Hussain (2014). Malik and Salahuddin (2015) obtained the numerical result of MHD viscous flow of a Williamson fluid by stagnation point towards a stretched cylinder. Krishnamurthy et al. (2016) scrutinized flow with MHD heat transfer of a Williamson liquid past a stretched sheet immersed in nanofluid with chemical reaction. The importance of the chemical reaction on three dimensional flow of a non-Newtonian Prandtl fluid over a Riga convectively-heated surface was discussed by Kumar et al. (2017a). Recently, Kumar et al. (2017b) considered the effect of nonlinear thermal radiation on non-Newtonian Williamson fluid comprising dusty particles suspended on stretched surface. Very recently, Kumar et al. (2018) scrutinized the influences of magnetic and thermal radiation effects on flow of hyperbolic tangent dusty fluid past a stretched surface.

Nowadays, the investigation of nanofluids has received admirable interest due to its various practical applications. Nanofluids are homogenous combination of nanoparticles and base or regular fluids similar to water, bio fluids, oil, ethylene glycol and other common liquids. Since the regular fluids have lower thermal conductivity which insufficient to assemble the necessity of today's rate of cooling. A dependable method to improve the thermal conductivity is to add in nanoparticles in regular fluid. Masuda et al. (1993) scattered the nanoparticles in fluid to enhance the thermal conductivity. Buongiorno (2006) observed that the thermophoresis diffusion and Brownian motion of nanoparticles give the immense enhancement in fluids thermal conductivity. Due to these effects, he suggested the modifications in the convective situations. Nield and Kuznetsov (2009, 2010) initially considered the flow along a vertical sheet with nanofluid. Later on, Khan and Pop (2010) expanded Nield and Kuznetsov work by considering a constant surface temperature comprising nanofluid over a stretched surface. The characteristics of heat transfer comprising nanoparticles towards a convectively-heated stretched sheet were examined by Makinde and Aziz (2011). They monitored that the characteristics of thermal can be considerably changed through mounting the effects of thermophoresis as well as Brownian motion. Rana and Bhargava (2012) inspected the steady flow holding nanoparticles past a non-linear stretched surface and obtained results numerically. Rashidi et al. (2013) considered electrically conducting flow containing nanoparticles using the second law of thermodynamics over a permeable rotating disk. The impact of heat generation on free convection flow containing nanofluid over a vertical surface immersed in non-Darcy medium was investigated by Chamkha et al. (2014). Beg et al. (2014) obtained the numerical results of single-phase and two-phase models in a circular tube filled with Al_2O_3-water based nanofluid. Garoosi et al. (2015) investigated free and mixed convective flow of a three types of nanofluid namely Cu, Al_2O_3 and

TiO_2 in a cavity. Abolbashari et al. (2015) explored the outcome of partial slip on flow of a non-Newtonian Casson nanofluid towards a convectively-heated stretched sheet with entropy generation and acquired the result via optimal homotopy technique. Free convective flow and heat exchangers in a cavity of nanofluid via Buongiorno model containing various heaters and coolers was scrutinized by Garoosi et al. (2015). Freidoonimehr et al. (2015) calculated MHD unsteady free convective flow of four different water-based nanofluids towards a porous vertical stretched sheet and obtained the numerical solution via the shooting method with RK technique. Rahman et al. (2016) investigated Brownian motion and thermophoresis diffusion using the second law of thermodynamics of a non-Newtonian Jeffrey nanofluid over a stretched sheet with zero flux. The characteristics of three dimensional MHD flow of a non-Newtonian Carreau fluid past a stretched surface containing nanoparticles in the presence of thermal radiation was explored by Rudraswamy et al. (2017). Krishnamurthy et al. (2018) discussed the impact of Al_2O_3-water nanoparticle on flow with heat transfer past a stretched surface embedded in a porous medium with thermal radiation holding dust particles. Recently, Hayat et al. (2018a) explored the influence of entropy generation on mixed convective flow of water-based silver and copper nanoparticles via a rotating disk in the presence of viscous dissipation, thermal radiation and Joule heating.

The study of boundary layer flow with non-linear radiation and convective condition is considered in several engineering and industrial processes involving die forging, thermal energy storage, chemical reactions, gas and nuclear turbines. Aziz (2009) inspected the flow towards a heated flat surface. Makinde and Aziz (2010) scrutinized mixed convective flow and MHD heat transfer past a vertical heated plate immersed in porous medium. Yao et al. (2011) obtained an exact result for viscous flow towards a porous convectively-heated stretched/shrinking wall. The

viscous flow with heat transfer towards a porous stretched surface through convective conditions was investigated numerically by Ishak (2014). The effect of nonlinear radiation on stagnation point flow of nanofluid towards a stretched sheet through convective condition was studied numerically by Mushtaq et al. (2014). Rahman et al. (2015) studied mixed convection flow over a vertical heated flat surface. Mustafa et al. (2015) investigated the steady flow a Maxwell fluid over a heated exponentially stretched sheet immersed in a nanofluid. Ibrahim and Haq (2016) studied the MHD flow holding nanoparticles near a stagnation-point over a heated stretched sheet. Makinde et al. (2016) scrutinized MHD stagnation-point flow past a connective heated stretched sheet by slip and radiation effects comprising nanofluid. Khan et al. (2016) deliberated the effect of nonlinear radiation on MHD flow of a Carreau fluid past a nonlinear stretched sheet with convective boundary condition. The thermal conductivity dependence on temperature near a stagnation-point towards a non-linear stretching sheet in the presence of variable thickness with Cattaneo-Christov heat flux was scrutinized by Hayat et al. (2016a). In another paper, Hayat et al. (2016b) discussed the influences of homogenous-heterogeneous reactions on stagnation-point flow of a Maxwell fluid past a stretched cylinder with Cattaneo-Christov heat flux. Mabood and Khan (2016) obtained the analytic solution of MHD unsteady flow over a convectively-heated stretched sheet holding nanoparticles. The influence of radiative flow on Oldroyd-B two-phase flow over a cone/wedge with Cattaneo–Christov heat flux was discussed by Reddy et al. (2018). Hayat et al. (2018b) discussed combined effects of Joule heating and viscous dissipation on radiative flow via a rotating disk in the presence of magnetic field.

The objective of the current research is to study the nonlinear radiative heat transfer on flow by dispersing nanoparticles into non-Newtonian Williamson fluid past a heated unsteady shrinking sheet. The transformed nonlinear differential equations are numerically solved via

shooting technique. Multiple solutions are obtained for accelerating flow and definite values of suction parameter. To the author's best of knowledge no one yet considered this type of problem. We expected that the present outcomes will give significant information for researchers. It is renowned that several devices meet flat or unexpected alteration in the environment of aerodynamic. The rotor of helicopter, the propeller of ship etc., normally operate in an unsteady environment.

2. Mathematical Formulation

Consider an unsteady nonlinear radiative flow of a non-Newtonian Williamson fluid towards a porous convectively-heated shrinking surface filled with nanoparticles. It is presumed that x, y axes measured along the shrinking surface and normal to it, respectively. It is also supposed that the velocity of surface is $u_w(x,t) = -ax/(1-ct)$ with $a(>0)$ and c are constants with dimensions $\mathbf{T^{-1}}$ (see Fig. 1). Further, it is assumed that at lower surface, the sheet was heated convectively with temperature T_f that offers a coefficient of heat transfer h_f. For Williamson fluid, the stress-tensor is specified as (Nadeem et al., 2013).

$$S = -pI + \tau, \tag{1}$$

and

$$\tau = \left(\mu_\infty + \frac{\mu_0 - \mu_\infty}{1 - \Gamma\dot{\gamma}}\right) A_1, \tag{2}$$

where τ, μ_0 and μ_∞ extra stress tensor, limiting viscosities at zero and infinite shear stress, respectively, $\Gamma > 0$ time constant, A_1 the first Rivilin-Erickson tensor and $\dot{\gamma}$ is described as

$$\dot{\gamma} = \sqrt{\frac{1}{2}\pi}, \quad \pi = \text{trace}\left(A_1^2\right). \tag{3}$$

Now, we only consider the case in which

$A_0 = 0$, $\varepsilon < 1$.

Thus, we get

$$\varsigma = \frac{A_0}{1-\varepsilon} A_1 \tag{4}$$

or using binomial expansion

$$\varsigma = A_0 \left(1+\varepsilon\right) A_1 \tag{5}$$

Under these assumptions, the physical equations that govern the unsteady flow are written as (Kumar et al. 2017b; Srinivas et al. 2017):

$$\frac{\partial u}{\partial x} + \frac{\partial v}{\partial y} = 0, \tag{6}$$

$$\frac{\partial u}{\partial t} + u\frac{\partial u}{\partial x} + v\frac{\partial u}{\partial y} = \nu \frac{\partial^2 u}{\partial y^2} + \sqrt{2}\nu\varepsilon \frac{\partial u}{\partial y}\frac{\partial^2 u}{\partial y^2}, \tag{7}$$

$$\frac{\partial T}{\partial t} + u\frac{\partial T}{\partial x} + v\frac{\partial T}{\partial y} = \alpha \frac{\partial^2 T}{\partial y^2} + \tau\left[D_B \frac{\partial C}{\partial y}\frac{\partial T}{\partial y} + \left(\frac{D_T}{T_\infty}\right)\left(\frac{\partial T}{\partial y}\right)^2 \right] - \frac{1}{(\rho c_p)_f}\frac{\partial q_r}{\partial y}, \tag{8}$$

$$\frac{\partial C}{\partial t} + u\frac{\partial C}{\partial x} + v\frac{\partial C}{\partial y} = D_B \frac{\partial^2 C}{\partial y^2} + \left(\frac{D_T}{T_\infty}\right)\left(\frac{\partial T}{\partial y}\right), \tag{9}$$

The boundary conditions are

$$\begin{aligned} t < 0 &: u = 0,\ v = 0,\ T = T_\infty,\ C = C_\infty \text{ for all } x, y \\ t \geq 0 &: u = u_w(x,t),\ v = -v_w(x,t),\ -k\frac{\partial T}{\partial y} = h_f(x,t)\left(T_f - T\right),\ C = C_w \text{ at } y = 0, \\ & u \to 0,\ T \to T_\infty,\ C \to C_\infty \text{ as } y \to \infty. \end{aligned} \tag{10}$$

where u, v velocity components in $x-$ and $y-$axes respectively, α the thermal diffusivity, ν the kinematic viscosity, ρ the density, T the temperature, T_∞ the free stream temperature, C the concentration of nanoparticles, D_B and D_T the coefficients of Brownian and thermophoresis

diffusion respectively, the ratio b/w the heat capacity and specific heat capacitance of nanoparticle material and fluid, $(\rho c_p)_f$ the specific heat capacitance of nanofluid.

Following Khan et al. (2016), the heat flux of radiative q_r is communicated as

$$q_r = -\frac{4\sigma}{3k}\frac{\partial T}{\partial y} = -\frac{16\sigma}{3k}T^3\frac{\partial T}{\partial y}, \tag{11}$$

where σ the constant of Stefan–Boltzmann and k the coefficient of mean absorption. Using Eq. (11), Energy eq. (8) can be written as

$$\frac{\partial T}{\partial t} + u\frac{\partial T}{\partial x} + v\frac{\partial T}{\partial y} = \frac{\partial}{\partial y}\left[\left(\alpha + \frac{16\sigma T^3}{3(\rho c_p)_f k}\right)\frac{\partial T}{\partial y}\right] + \tau\left[D_B\frac{\partial C}{\partial y}\frac{\partial T}{\partial y} + \left(\frac{D_T}{T_\infty}\right)\left(\frac{\partial T}{\partial y}\right)^2\right]. \tag{12}$$

Now, we introduce the similarity transformation (Naganthran et al., 2016):

$$\eta = y\sqrt{\frac{a}{\nu(1-ct)}},\ \psi = \sqrt{\frac{a\nu}{(1-ct)}}xf(\eta),\ \theta(\eta) = \frac{T-T_\infty}{T_f-T_\infty},\ \phi(\eta) = \frac{C-C_\infty}{C_w-C_\infty}. \tag{13}$$

Here η, ψ the similarity variable and the stream function, respectively. We get $T = T_\infty\left[1+(\theta_w-1)\theta\right]$ with $\theta_w > 1$, where $\theta_w = T_f/T_\infty$ being the temperature ratio parameter. Here for similarity solution, we assumed that $T_f = T_1(1-ct)^{3/2}/x$ (see Naganthran et al., 2016), $v_w(t) = v_0/\sqrt{1-ct}$ the variable velocity of suction with v_0 a positive constant and $h_f(t) = d/\sqrt{1-ct}$ with $d > 0$ (see Mahapatra and Nandy, 2013).

In view of relation (13), equation (7)-(12) are transmuted into ODEs

$$f''' + ff'' - f'^2 + \delta f''f''' - A\left(f' + \frac{1}{2}\eta f''\right) = 0, \tag{14}$$

$$\theta'' + \Pr f\theta' + \frac{4}{3R_d}\frac{d}{d\eta}\left[\left\{1+(\theta_w-1)\theta\right\}^3\theta'\right] + \Pr\left[Nb\theta'\phi' + Nt(\theta')^2\right] - \frac{1}{2}\Pr A\eta\theta' = 0, \tag{15}$$

$$\phi''+Scf\phi'+\frac{Nt}{Nb}\theta''-\frac{1}{2}\Pr ScA\eta\phi'=0, \tag{16}$$

subject to the boundary conditions

$$\begin{aligned} &f(0)=S,\ f'(0)=-1,\ \theta'(0)=-\gamma\left(1-\theta(0)\right),\ \phi(0)=1,\\ &\quad f'(\infty)\to 0,\ \theta(\infty)\to 0,\ \phi(\infty)\to 0. \end{aligned} \tag{17}$$

where prime signify differentiation w.r.t η, $\delta=\sqrt{2}\Gamma_1 a^{3/2}/\sqrt{\nu}$ the non-Newtonian Williamson parameter, $A=c/a$ an unsteady parameter, $\Pr=$ the Prandtl number, $Nb=D_B\left(C_w-C_\infty\right)/$ the Brownian motion parameter, $Nt=D_T\left(T_f-T_\infty\right)/T_\infty$ the thermophoresis parameter, $\gamma=d\sqrt{a}/k$ the convective parameter, $R_d=/4$ the thermal radiation parameter, $S=v_0/\sqrt{a}>0$ the suction parameter and $Sc=/D_B$ the Schmidt number.

The vital physical quantities are the skin friction coefficient, the Nusselt number and the Sherwood Number are defined as

$$C_f=\frac{}{\rho}, \quad Nu_x=-\frac{}{k(T_f-T_w)}, \quad Sh=\frac{}{D_B(C_w-C_\infty)}, \tag{18}$$

where $,,$ the shear stress in $-$ direction, the heat flux and the mass flux, respectively given as

$$=\mu_0\left(\frac{\partial}{\partial}+\frac{\Gamma}{\sqrt{2}}\left(\frac{\partial}{\partial}\right)^2\right)_{=0},\ =-k\left(\frac{\partial T}{\partial}\right)_w+\left(\right)_w,\ =-D_B\left(\frac{\partial C}{\partial}\right)_{=0}, \tag{19}$$

Using (13), we get

$$\begin{aligned} &C_f\,\mathrm{Re}_x^{1/2}=f''(0)+\frac{\delta}{2}\left(f''(0)\right)^2,\ \ Sh_x\,\mathrm{Re}_x^{-1/2}=-\phi'(0),\\ &Nu_x\,\mathrm{Re}_x^{-1/2}=-\left[1+\frac{4}{3R_d}\left\{1+\left(\theta_w-1\right)\theta(0)\right\}^3\right]\theta'(0). \end{aligned} \tag{20}$$

where $\mathrm{Re}_x = \rho_w (\quad) / \quad$ is the Reynolds number.

3. Methodology

In the present research, a useful numerical technique namely the shooting method has been utilized to scrutinize the flow problem described by the transformed equations (14)-(17). The summary of this method is given below in following steps:

First, convert the equations (14)-(17) into IVP (initial value problem). Then select a suited finite value of $\eta \to \infty$, say η_∞. We have the set of following first-order system

$$\left.\begin{aligned} f' &= p, \\ p' &= q, \\ q' &= \left(p^2 - fq - 1 - K(1-p) - \lambda\theta\right) / \Lambda\left(1 + \frac{1}{\beta_1}\right), \end{aligned}\right\} \tag{21}$$

$$\left.\begin{aligned} \theta' &= z, \\ z' &= \begin{pmatrix} -\Pr fz - \frac{4}{R_d}(\theta_w - 1)\left\{1 + (\theta_w - 1)\theta\right\}^2 z^2 \\ -\Pr\left(Nbzm + Ntz^2\right) + \frac{1}{2}\Pr A\eta z \end{pmatrix} \Big/ \left(1 + \frac{4}{3R_d}\left\{1 + (\theta_w - 1)\theta\right\}^3\right), \end{aligned}\right\} \tag{22}$$

$$\left.\begin{aligned} \phi' &= m, \\ m' &= -Scfm - \frac{Nt}{Nb} z' + \frac{1}{2} ScA\eta m, \end{aligned}\right\} \tag{23}$$

under the boundary conditions

$$f(0) = S,\ p(0) = -1,\ z(0) = -\gamma\left(1 - \theta(0)\right), \phi(0) = 1. \tag{24}$$

To solve the system of equations as an IVP, we require the values for $q(0)$ i.e. $f''(0)$, $z(0)$ i.e. $\theta'(0)$ and $m(0)$ i.e. $\phi'(0)$; however no such values are specified. The values of the initial guesses for $f''(0)$, $\theta'(0)$ and $\phi'(0)$ are chosen and the Runge–Kutta fourth-order method is

executed to acquire a solution. Then the calculated values of $f'(\eta)$, $\theta(\eta)$ and $\phi(\eta)$ at η_∞(=8) are compared under the known boundary conditions $f'(\eta_\infty)=0$, $\theta(\eta_\infty)=0$ and $\phi(\eta_\infty)=0$. The step size is taken as $\Delta\eta=0.01$. The technique is repeated until we obtain results correct up to the desired accuracy of the 10^{-5} level, which fulfills the convergence criterion.

4. Results and discussion

Tables 1 and 2 show the assessment of our results of $-f''(0)$ and $-\theta'(0)$, respectively with those available results in literature. As noticed an excellent match with the published ones up to a significant number of digits has been obtained.

The velocity, temperature distribution and the concentration of nanoparticles for different values of the non-Newtonian Williamson parameter δ are depicted in Figs. 2-4. From Fig. 2, the velocity explains a diminishing development for growing values of δ in the first solution and thus, the momentum boundary layer thickness increases, while the velocity enhances and the boundary thickness decreases in the second solution. In contrast, the temperature distribution and the concentration of nanoparticles show an increasing behavior with increasing values of δ for the first solution as portrayed in Figs. 3 and 4 and consequently, the thermal and concentration boundary layers thicknesses boost. On the other hand, for the second solution, the reverse trend is observed. It is also witnessed from these portrays that the velocity, temperature distribution and the concentration of nanoparticles are larger for a non-Newtonian Williamson fluid compared with a Newtonian fluid $(\delta=0)$ for the first solution.

Figures 5-7 preserve the variation of unsteady parameter A on the velocity of fluid, temperature distribution and concentration of nanoparticles. Fig. 5 indicates an increasing trend in velocity field with rising values of A in the first solution and in the second solution the profile indicates an opposite behavior. Further, it is also perceived from this portray that the velocity

initially increases with increasing η for first solution and after a certain value of $\eta = 1$, it starting decreases. The unsteady effect is major in the lower branch solution (second solution) compared to upper branch solution (First solution). The temperature distribution and concentration profile increase with increasing A for first and second solutions as shown in Figs. 6 and 7, respectively. Thus the thermal and concentration boundary layers thicknesses increase for both solutions. Further, these sketches fulfill asymptotically the boundary conditions and the existence of multiple solutions that support the validation of our obtained numerical results.

Fig. 8 shows that due to mounting values of the Brownian parameter Nb, the temperature distribution raises in first and second solutions, whereas the conflicting behavior is noticed for the concentration of nanoparticle as revealed in Fig. 9. Thus, the thermal boundary layer thickness increases, while the concentration boundary layer thickness shrinks. This is because of the kinetic energy of the nanoparticles increases due to the strength of this chaotic motion and as a result, the fluids temperature increases. This is because the Brownian motion at nanoscale and molecular levels is an important mechanism of the nanoscale level that governs the thermal behaviors. In systems using nanofluids, the Brownian motion captures place because of the nanoparticles size which can change the properties of heat transfer. As the scale size of particles advances to the scale of nanometer, the particles Brownian motion and its result on the surrounding fluids play a vital role in heat transfer characteristics. Figures 10 and 11 preserve the influence of the thermophoresis parameter Nt on the temperature distribution and concentration profile. These figures illustrate that the temperature and concentration profiles show an increasing trend for increasing values of Nt for first as well as for second solutions. This is because diffusion penetrates deeper into the fluid due to increasing values of Nt which causes the thickening of the thermal boundary layer as well as the concentration boundary layer.

The effects of the convective parameter γ on the temperature distribution and concentration of nanoparticles are depicted in Figs. 12 and 13, respectively. Fig. 12 reveals that due to increase in the value of γ resulting from the powerful convective heating at the surface, the temperature gradient at the surface of sheet increases. This permits the effect of thermal to enter deeper into the quiescent fluid. Therefore, the temperature as well as the thermal boundary layer thickness enhances with rising values of γ for first and second solutions. It is worth mentioning that the constant wall temperature $\theta(0)=1$ can be recovered by taking sufficiently large values of the convective parameter. Further $\gamma=0$ communicates an insulated surface case. Fig. 13 confirms that the concentration of nanoparticles and the boundary layer thickness increase with γ in first and second solutions. Figs. 14 and 15 are prepared to illustrate the impact of radiation R_d on temperature distribution and concentration nanoparticles. These figures showed a decreasing behavior for increasing R_d in first and second solutions. Thus, the thermal and concentration boundary layers thicknesses become thinner and thinner in both forms. Since huge value of the radiation means the conduction dominance and thus, the thermal and concentration boundary layers thicknesses decrease. The impact of radiation is more pronounced on temperature distribution compared to concentration profile. In Fig. 16, the Schmidt number effect on the concentration of nanoparticles is shown. As expected the graph and the boundary layer thickness shrinks with enhancing Sc in first and second solutions.

The impact of the non-Newtonian Williamson fluid parameter δ versus A on the skin friction, the local Nusselt number and the Sherwood number are shown in Figs. 17-19. It can be seen that multiple solutions of the similarity equations (14)-(16) subjected to (17) exist in decelerating flow ($A\le 0$) (see Mahapatra and Nandy, 2013), while for accelerating flow ($A>0$

), the solution is unique. On the other hand, the dual solutions are obtained for $A \geq A_c$ and the flow has no solution for $A < A_c$, where A_c is the critical value of A. For $\delta = 0$ (Newtonian fluid), the critical point looks far from negative region, so we stopped calculation at $A = -10$. This is consistent with the results obtained in References (Ali et al., 2011; Rohni, 2012). For $\delta = 0.3$, the dual solutions exist for ranges of A is $A \geq -1.9700$ and thus no solution exists for $A < -1.9700$. It is worth mentioning that more amount of non-Newtonian parameter δ causes remarkable reduction $\left(|A_c|\right)$ in the solution domain. For $\delta = 0.5$, the solution exists when $A \geq -1.0000$ and therefore no solution exists for $A < -1.0000$. Thus it can be concluded that the critical point $\left(|A_c|\right)$ reduces when non-Newtonian parameter increases which delays the boundary layer separation. Further, due to increasing values of δ, the skin friction, the local Nusselt number and the Sherwood number decrease for the first solution and increases in case of second solution as illustrated in Figs. 17-19.

The values $C_f \, \mathrm{Re}_x^{1/2}$, $Nu_x \, \mathrm{Re}_x^{-1/2}$ and $Sh_x \, \mathrm{Re}_x^{-1/2}$ versus S for several values of the unsteady parameter A are illustrated in Figs. 20-22, respectively and in Table 3. Fig. 20 reveals that the skin friction enhances with increasing A for first as well as for second solutions. In contrast, the values of the Nusselt number and the Sherwood number decrease with increasing A for first and second solutions as shown in Figs. 21 and 22. The behavior of these results also can be seen through Table 2. Dual solutions are achieved for $S \geq S_c$ and no solution for $S < S_c$ where S_c is the critical value of S. Further, the impact of A towards a critical value has been shown in Table 4. The larger characteristics of unsteady parameter decrease the values of critical point. Thus the unsteady parameter delays the boundary layer separation.

Figs. 23 and 24 confirm the deviations of the Nusselt number $Nu_x \mathrm{Re}_x^{-1/2}$ and the Sherwood number $Sh_x \mathrm{Re}_x^{-1/2}$ versus S for different values of the Brownian motion parameter Nb. These results prove that the values of the Nusselt number decreases and the Sherwood number raises with enlarging Nb in the first and the second solutions. These results are consistent with the results obtained by Rana and Bhargava (2012) in case of a nonlinearly-stretching sheet. Therefore, by using the Brownian motion, the thermal conduction can be increased either by taking straight outcome due to nanoparticles that transport heat or by taking indirect micro-convection of the surrounding fluid individual nanoparticles. Further, the smaller values of Nb indicate that the Brownian motion is weak for the small particles and for larger values of Nb it shows the opposite behavior.

5. Conclusions

In this research, we have investigated unsteady boundary layer flow of non-Newtonian Williamson nanofluid over a convectively-heated shrinking sheet with a nonlinear thermal radiation. The transformed ordinary differential equations were numerically solved via the shooting technique for several values of the pertinent parameters. The main findings are:

- Multiple results are achieved for some values of the suction and for decelerating flow only.
- Due to the non-Newtonian parameter, the velocity of the fluid decreases in the first solution and increases in the second solution. On the other hand, the temperature and concentration profiles increase and decrease in the first and the second solutions, respectively.
- Initially, the velocity distribution shows an increasing behavior and then it starts to decrease due to increasing values of the unsteady parameter for both solutions, while the temperature and concentration profiles confirm an increasing behavior in both solutions.

- The thermal and concentration boundary layer thicknesses develop due to the convective parameter for the first and the second solutions.
- The thermal radiation reduces the temperature of the fluid as well as the concentration profile for both solutions.
- Using the Brownian motion mechanism, the distribution of the nanoparticles could be arranged in the flow regime by taking larger values of Nb or Nt and also cooling of regime could be achieved by taking smaller values of Nb or Nt.
- The unsteady parameter and the non-Newtonian parameter delay the boundary layer separation.

References

Abolbashari, M.H., Freidoonimehr, N., Nazari, F. and Rashidi, M.M. (2015) "Analytical modeling of entropy generation for Casson nano-fluid flow induced by a stretching surface", *Advanced Powder Tech*. Vol. 26, pp. 542–552.

Ali, F.M., Nazar, R., Arifin, N.M. and Pop, I. (2011), "Unsteady flow and heat transfer past an axisymmetric permeable shrinking sheet with radiation effect", *Int. J. Numer. Meth. Fluids*, Vol. 67, pp. 1310–1320.

Aziz, A. (2009), "A similarity solution for laminar thermal boundary layer over a flat plate with a convective surface boundary condition", *Commun. Nonlinear Sci. Numer. Simul*. Vol. 14, pp. 1064–1068.

Beg, O.A. Rashidi, M.M., Akbari, M. and Hosseini, A. "Comparative numerical study of single-phase and two-Phase models for bio-nanofluid transport phenomena", *J. Mech. Medicine Biology*, Vol. 14, pp. 1–31.

Buongiorno, J. (2006), "Convective transport in nanofluids", *ASME J. Heat Transfer*, Vol. 128, pp. 240–250.

Chamkha, A.J., Aly, A.M., Mansour, M.A. (2010), "Similarity solution for unsteady heat and mass transfer from a stretching surface embedded in a porous medium with suction/injection and chemical reaction effects", *Chem. Eng. Commun*. Vol. 197, pp. 846–858.

Chamkha, A.J., Rashad, A.M., Ram Reddy, Ch. and Murthy, P.V.S.N. (2014), "Effect of suction/ injection on free convection along a vertical plate in a nanofluid saturated non-Darcy porous medium with internal heat generation", *Indian J. Pure Appl. Math*. Vol. 45, pp. 321–342.

Freidoonimehr, N., Rashidi, M.M. and Mahmud, S. (2015), "Unsteady MHD free convective flow past a permeable stretching vertical surface in a nano-fluid", *Int. J. Thermal Sci*., Vol. 87, pp. 136–145.

Garoosi, F. Bagheri, G. and Rashidi, M.M. (2015), "Two phase simulation of natural convection and mixed convection of the nanofluid in a square cavity", *Powder Technology*, Vol. 275, pp. 239–256.

Garoosi, F., Jahanshaloo, L., Rashidi, M.M., Badakhsh, A. and Ali, M.A. (2015), "Numerical simulation of natural convection of the nanofluid in heat exchangers using a Buongiorno model", Appl. Math. Comput. Vol. 254, pp. 183–203.

Hayat, T., Ijaz Khan, M., Farooq, M., Alsaedi, A., Waqas, M. and Yasmeen, T. (2016a), "Impact of Cattaneo–Christov heat flux model in flow of variable thermal conductivity fluid over a variable thicked surface", *Int. J. Heat Mass Transfer*, Vol. 99, pp. 702–710.

Hayat, T., Ijaz Khan, M., Farooq, M., Yasmeen, T. and Alsaedi, A. (2016b), "Stagnation point flow with Cattaneo-Christov heat flux and homogeneous-heterogeneous reactions", *J. Mol. Liq*., Vol. 220, pp. 49–55.

Hayat, T., Ijaz Khan, M., Qayyum, S. and Alsaedi, A. (2018a), "Entropy generation in flow with silver and copper nanoparticles", *Col. Surf. A: Physicochem. Eng. Aspects*, Vol. 539, pp. 335–346.

Hayat, T., Qayyum, S., Ijaz Khan, M. and Alsaedi, A. (2018b), "Entropy generation in magnetohydrodynamic radiative flow due to rotating disk in presence of viscous dissipation and Joule heating", *Phys. Fluids*, Vol. 30, 017101.

Ibrahim, W. and Haq, R.U. (2016), "Magnetohydrodynamic (MHD) stagnation point flow of nanofluid past a stretching sheet with convective boundary condition", *J. Braz. Soc. Mech. Sci. Eng*. Vol. 38, pp. 1155–1164.

Ishak, A. (2014), "Similarity solutions for flow and heat transfer over a permeable surface with convective boundary condition", *Appl. Math. Comp*. Vol. 217, pp. 837–842.

Khan, N.A. and Khan, H.A. (2014), "Boundary layer flows of non-Newtonian Williamson fluid", *Nonlinear Eng*. Vol. 3, pp. 107–115.

Khan, W.A. and Pop, I. (2010), "Boundary-layer flow of a nanofluid past a stretching sheet", *Int. J. Heat Mass Transfer*, Vol. 53, pp. 2477–2483.

Khan, M., Hashim, Hussain, M. and Azam, M., (2016), "Magnetohydrodynamic flow of Carreau fluid over a convectively heated surface in the presence of non-linear radiation", *J. Magn. Magn. Mater*. Vol. 412, pp. 63–68.

Krishnamurthy, M.R., Kumar, K.G., Gireesha, B.J. and Rudraswamy, N.G. (2018), "MHD flow and heat transfer (PST and PHF) of dusty fluid suspended with alumina nanoparticles over a stretching sheet embedded in a porous medium under the influence of thermal radiation", *J. Nanofluid*, Vol. 7, No. 3, pp. 527–535.

Krishnamurthy, M.R., Prasannakumara, B.C., Gireesha, B.J. and Gorla, R.S.R. (2016) "Effect of chemical reaction on MHD boundary layer flow and melting heat transfer of Williamson nanofluid in porous medium", *Eng. Sci. Tech. Int. J*. Vol. 19, pp. 53–61.

Kumar, K.G., Gireesha, B.J. and Gorla, R.S.R. (2018), "Flow and heat transfer of dusty hyperbolic tangent fluid over a stretching sheet in the presence of thermal radiation and magnetic field", *Int. J. Mech. Mater. Eng*., Vol. 13, No. 2, pp. 1–11.

Kumar, K.G., Rudraswamy, N.G., Gireesha, B.J. and Manjunatha, S. (2017b), "Non linear thermal radiation effect on Williamson fluid with particle-liquid suspension past a stretching surface", *Results Phys*., Vol. 7, pp. 3196–3202.

Kumar, K.G., Haq, R.U., Rudraswamy, N.G. and Gireesha, B.J. (2017a), "Effects of mass transfer on MHD three dimensional flow of a Prandtl liquid over a flat plate in the presence of chemical reaction", *Results Phys*., Vol. 7, pp. 3465–3471.

Mabood, F. and Khan, W.A. (2016), "Analytical study for unsteady nanofluid MHD Flow impinging on heated stretching sheet", J. Mol. Liq. Vol. 219, pp. 216–223.

Mahapatra, T.R. and Nandy, S.K. (2013), "Slip effects on unsteady stagnation-point flow and heat transfer over a shrinking sheet", Meccanica, Vol. 48, pp. 1599–1606.

Makinde, O.D. and Aziz, A. (2010), "MHD mixed convection from a vertical plate embedded in a porous medium with a convective boundary condition", *Int. J. Thermal Sci*. Vol. 49, pp. 1813–1820.

Makinde, O.D. and Aziz, A. (2011), "Boundary layer flow of a nanofluid past a stretching sheet with a convective boundary condition", *Int. J. Thermal Sci*. Vol. 50, pp. 1326–1332.

Makinde, O.D., Khan, W.A. and Khan, Z.H. (2016), "Stagnation point flow of MHD chemically reacting nanofluid over a stretching convective surface with slip and radiative heat", *Proc. IMechE Part E: J. Process Mech. Eng*. Vol. 0, pp. 1–9.

Malik, M.Y. and Salahuddin, T. (2015), "Numerical solution of MHD stagnation point flow of Williamson fluid model over a stretching cylinder," *Int. J. Nonlinear Sci. Num. Simul*. 16 (2015) 161–164.

Masuda, H., Ebata, A., Teramae, K. and Hishinuma, N. (1993), "Alteration of thermal conductivity and viscosity of liquid by dispersing ultra-fine particles", *Netsu Bussei*, Vol. 7, pp. 227–233.

Mushtaq, A., Mustafa, M., Hayat, T. and Alsaedi, A. (2014), "Nonlinear radiative heat transfer in the flow of nanofluid due to solar energy: A numerical study", *J. Taiwan Institute Chem. Eng*. Vol. 45, pp. 1176–1183.

Mustafa, M., Khan, J.A., Hayat, T. and Alsaedi, A. (2015), "Simulations for Maxwell fluid flow past a convectively heated exponentially stretching sheet with nanoparticles", *AIP Advances*, Vol. 5, pp. 037133.

Nadeem, S., Hussain, S.T. and Lee, C. (2013), "Flow of a Williamson fluid over a stretching sheet", *Braz. J. Chem. Eng*. Vol. 30, pp. 619–625.

Nadeem, S. and Hussain, S.T. (2014), "Heat transfer analysis of Williamson fluid over exponentially stretching surface", *Appl. Math. Mech. -Engl. Ed.* Vol. 35, pp. 489–502.

Naganthran, K., Nazar, R. and Pop, I. (2016), "Unsteady stagnation-point flow and heat transfer of a special third grade fluid past a permeable stretching/shrinking sheet", *Scientific Reports*, Vol. 6, pp. 24632.

Nield, D.A. and Kuznetsov, A.V. (2009), "The Cheng–Minkowycz problem for natural convective boundary-layer flow in a porous medium saturated by a nanofluid", *Int. J. Heat Mass Transfer*, Vol. 52, pp. 5792–5795.

Nield, D.A. and Kuznetsov, A.V. (2010), "Natural convective boundary-layer flow of a nanofluid past a vertical plate", *Int. J. Thermal Sci*. Vol. 49, pp. 243–247.

Rahman, M.M., Merkin, J.H. and Pop, I. (2015), "Mixed convection boundary-layer flow past a vertical flat plate with a convective boundary condition", *Acta Mech*. Vol. 226, pp. 2441–2460.

Rehman, S.U., Haq, R.U., Khan, Z.H. and C. Lee, (2016), "Entropy generation analysis for non-Newtonian nanofluid with zero normal flux of nanoparticles at the stretching surface", *J. Taiwan Instit. Chem. Eng*. Vol. 63, pp. 226–236.

Rana, P. and Bhargava, R. (2012), "Flow and heat transfer of a nanofluid over a nonlinearly stretching sheet: A numerical study", *Commun. Nonlin. Sci. Num.Simul*. Vol. 17, pp. 212–226.

Rashidi, M.M., Abelman, S. and Freidoonimehr, N. (2013), "Entropy generation in steady MHD flow due to a rotating porous disk in a nanofluid", *Int. J. Heat Mass Transfer*, Vol. 62, pp. 515–525.

Reddy, M.G., Sudha Rani, M.V.V.N.L., Ganesh Kumar, K. and Prasannakumara, B.C. (2018), "Cattaneo–Christov heat flux and non-uniform heat-source/sink impacts on radiative Oldroyd-B two-phase flow across a cone/wedge", *J. Brazilian Soc. Mech. Sci. Eng*., Vol. 40, No. 2, pp. 1–21.

Rohni, A.M. (2012), "Flow over an unsteady shrinking sheet with suction in a nanofluid", *International Conference Mathematical and Computational Biology*, Vol. 9, pp. 511–519.

Rudraswamy, N.G., Shehzad, S.A., Ganesh Kumar, G. and Gireesha, B.J. (2017), "Numerical analysis of MHD three-dimensional Carreau nanoliquid flow over bidirectionally moving surface", *J. Braz. Soc. Mech. Sci. Eng*., Vol. 39, No. 2, pp. 5037–5047.

Shafie, S., Mahmood, T. and Pop, I. (2006), "Similarity solutions for the unsteady boundary layer flow and heat transfer due to a stretching sheet", *Int. J. Appl. Mech. Eng*. Vol. 11, pp. 647–654.

Srinivas, R.C, Naikoti, K. and Rashidi, M.M. (2017), "MHD flow and heat transfer characteristics of Williamson nanofluid over a stretching sheet with variable thickness and variable thermal conductivity", *Tran. A. Razmadze Math. Inst*., Vol. 171, pp. 195–211.

Williamson, R.V. (1929), "The flow of pseudoplastic materials", *Industrial Eng. Chem. Res*. Vol. 21, pp. 1108–1111.

Yao, S., Fang, T. and Zhong, Y. (2011), "Heat transfer of a generalized stretching/shrinking wall problem with convective boundary conditions", *Commun. Nonlinear Sci. Numer. Simul*. Vol. 16, pp. 752–760.

Table 1: Comparison of $-f''(0)$ when $\delta = 0$ (Newtonian fluid), $S = 0$ in case of stretching sheet $f'(0) = 1$.

A	Sharidan et al. (2006)	Chamkha et al. (2010)	Present
0.8	1.261042	1.261512	1.2610
1.2	1.377722	1.378052	1.3777

Table 2: Comparison of $-\theta'(0)$ when $\delta = 0$ (Newtonian fluid), $S = 0$, $R_d \to \infty$, $\Pr = 10$, $Sc = 10$, $\gamma = 0.1$ in case of stretching sheet $f'(0) = 1$.

Nt	Nb	Makinde and Aziz (2011)	Present
0.1	0.1	0.0929	0.0929
	0.2	0.0873	0.0873
0.2	0.1	0.0927	0.0927
	0.2	0.0868	0.0868

0.3	0.1	0.0925	0.0925
	0.2	0.0861	0.0861
0.4	0.1	0.0923	0.0923
	0.2	0.0854	0.0854
0.5	0.1	0.0921	0.0921
	0.2	0.0845	0.0845

Table 3: Values of skin friction, Nusselt number and Sherwood number versus S for different values of A when $\delta = 0.3,\ Nb = 1,\ Nt = 1.5,\ Sc = 1,\ Q_w = 1.5,\ R_d = 2,\ \gamma = 0.3$ are fixed.

S	A	$C_f \operatorname{Re}_x^{1/2}$		$Nu_x \operatorname{Re}_x^{-1/2}$		$Sh_x \operatorname{Re}_x^{-1/2}$	
		First solution	Second solution	First solution	Second solution	First solution	Second solution
2.8	-1	2.0069	-1.6142	1.0911	1.0837	2.0890	1.7582
	-0.5	2.1436	-0.9050	1.0889	1.0785	1.9692	1.5839
	-0.2	2.2258	-0.3232	1.0871	1.0733	1.8844	1.4394
2.4	-1	1.3650	-0.5630	1.0833	1.0762	1.7062	1.5043
	-0.5	1.5551	-0.1125	1.0788	1.0673	1.5666	1.3116
	-0.2	1.6687	0.2284	1.0748	1.0570	1.4615	1.1399
2.2	-1	0.8513	0.0694	1.0765	1.0725	1.4969	1.4049
	-0.5	1.1381	0.3225	1.0696	1.0614	1.3469	1.2109
	-0.2	1.3010	0.5207	1.0630	1.0482	1.2278	1.0344

Table 4: Critical values of S_c for different values of A when $\delta = 0.3,\ Nb = 1,\ Nt = 1.5,\ Sc = 1,$ $Q_w = 1.5,\ R_d = 2,\ \gamma = 0.3$ are fixed.

A	S_c
-1	2.1528

-0.5	2.1229
-0.2	2.0990

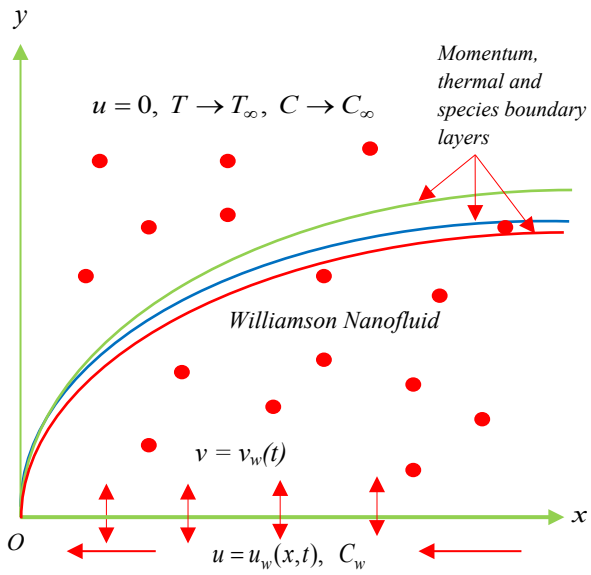

Figure 1: Sketch c $-k\frac{\partial T}{\partial y} = h_f(t)\left(T_f - T\right)$ v problem.

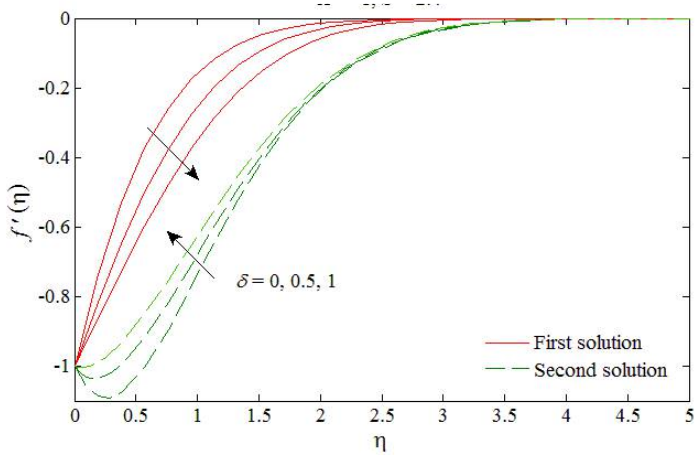

Figure 2: The velocity profiles for different values of δ.

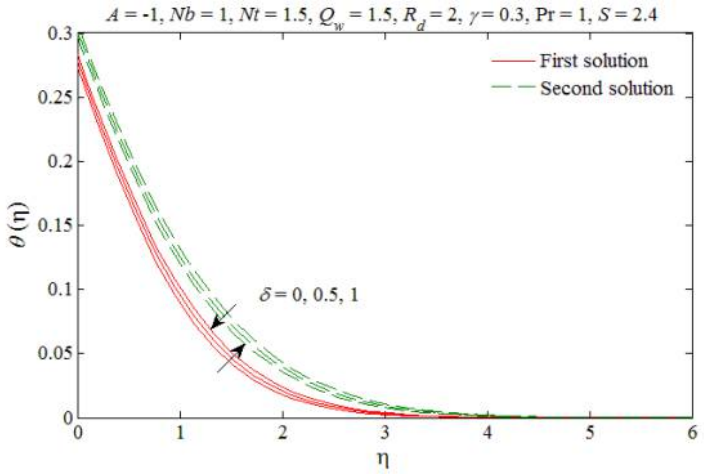

Figure 3: The temperature profiles for different values of δ.

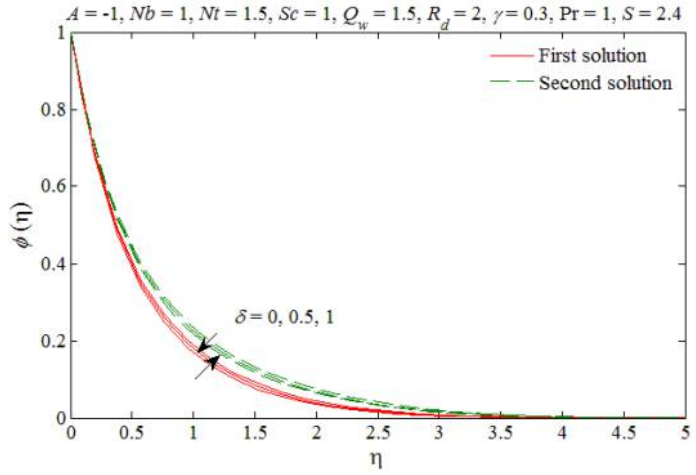

Figure 4: The concentration profiles for different values of δ.

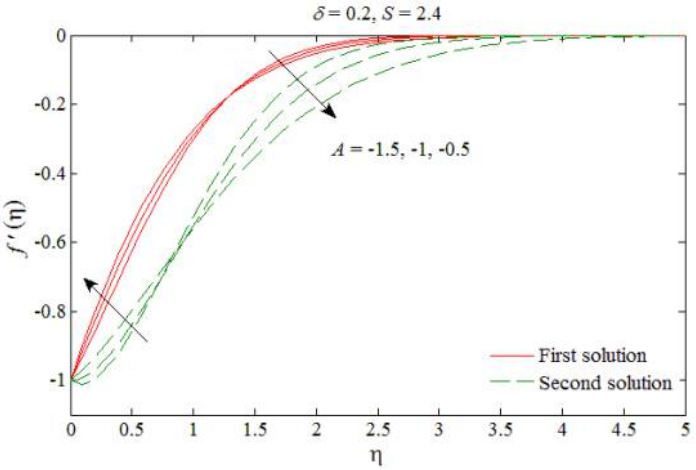

Figure 5: The velocity profiles for different values of A.

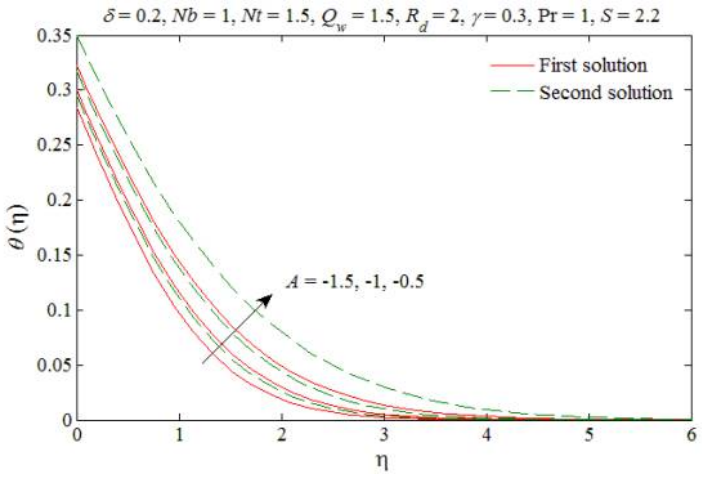

Figure 6: The temperature profiles for different values of A.

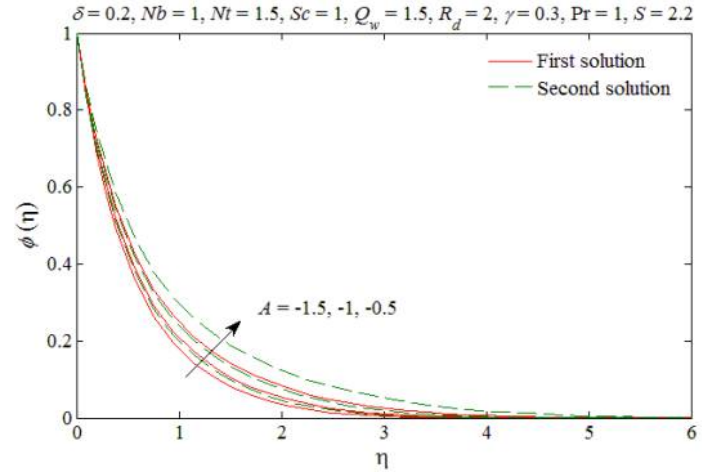

Figure 7: The concentration profiles for different values of A.

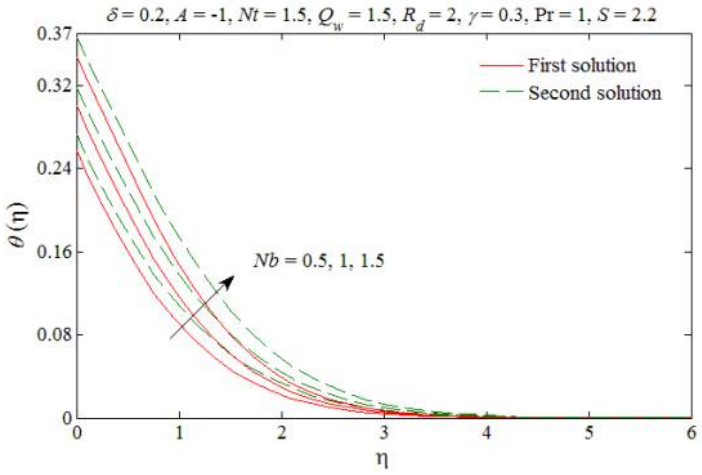

Figure 8: The temperature profiles for different values of Nb.

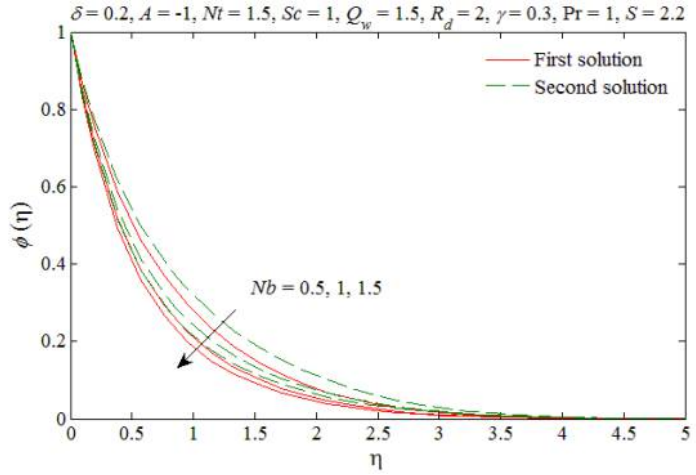

Figure 9: The concentration profiles for different values of Nb.

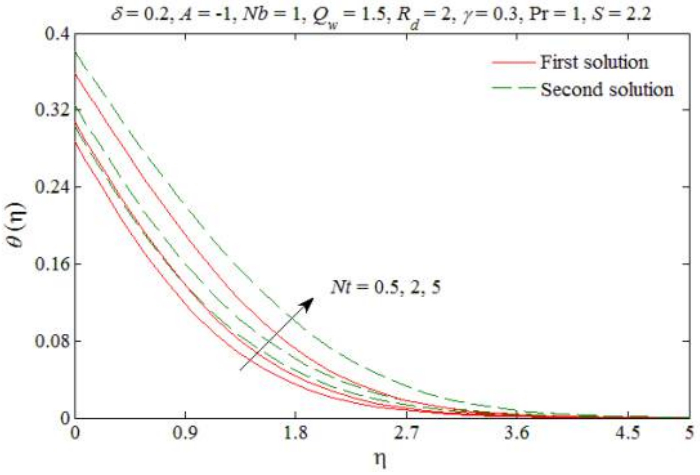

Figure 10: The temperature profiles for different values of Nt.

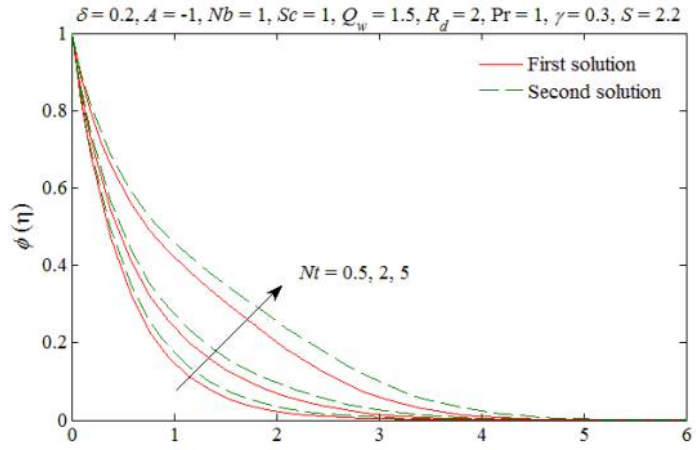

Figure 11: The concentration profiles for different values of Nt.

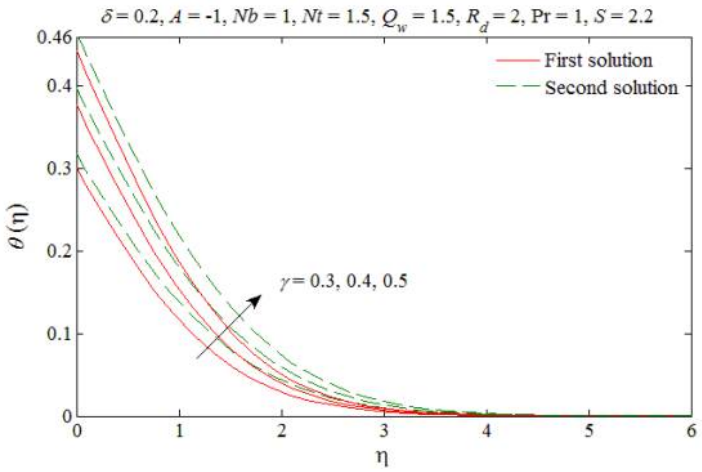

Figure 12: The temperature profiles for different values of γ.

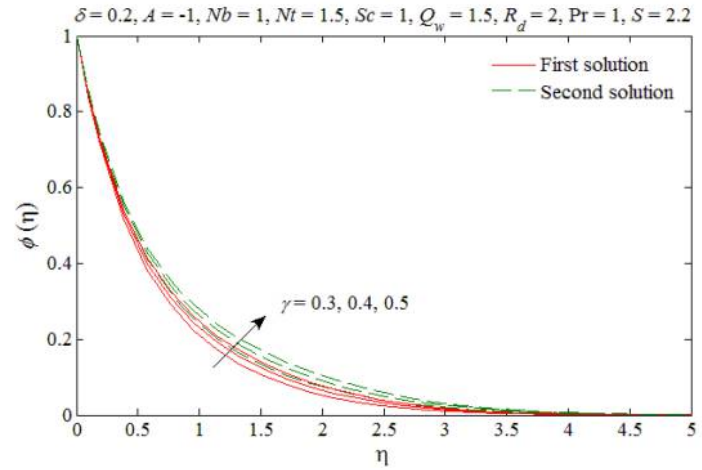

Figure 13: The concentration profiles for different values of γ.

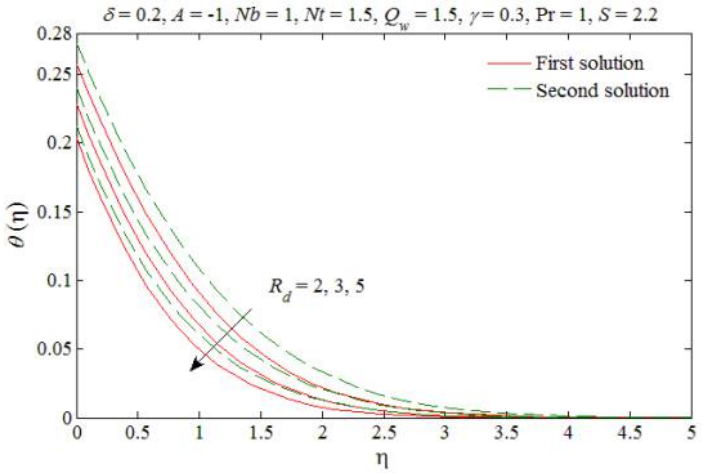

Figure 14: The temperature profiles for different values of R_d.

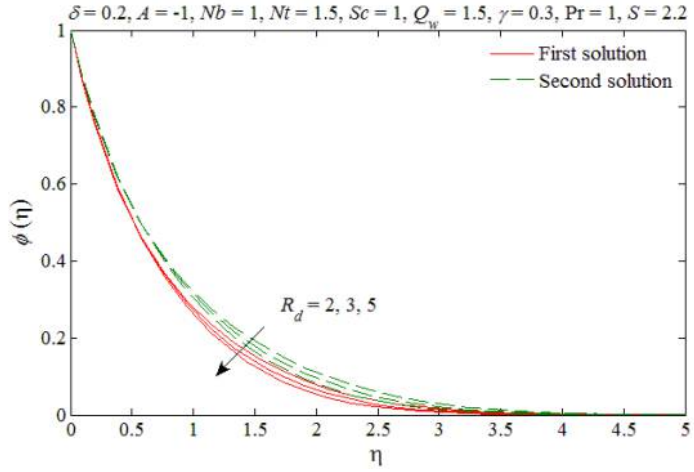

Figure 15: The concentration profiles for different values of R_d .

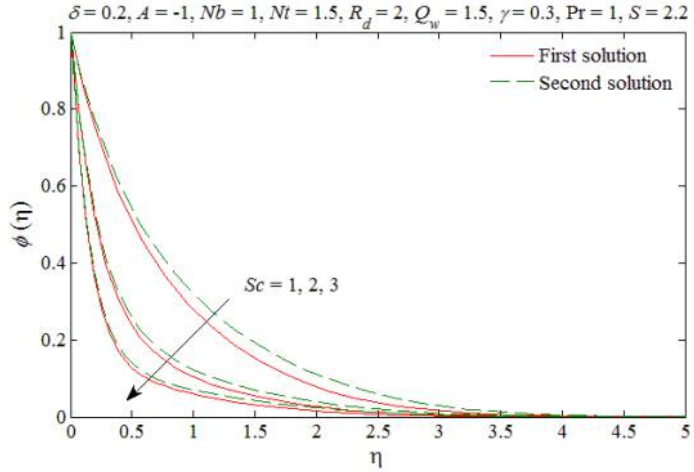

Figure 16: The concentration profiles for different values of Sc .

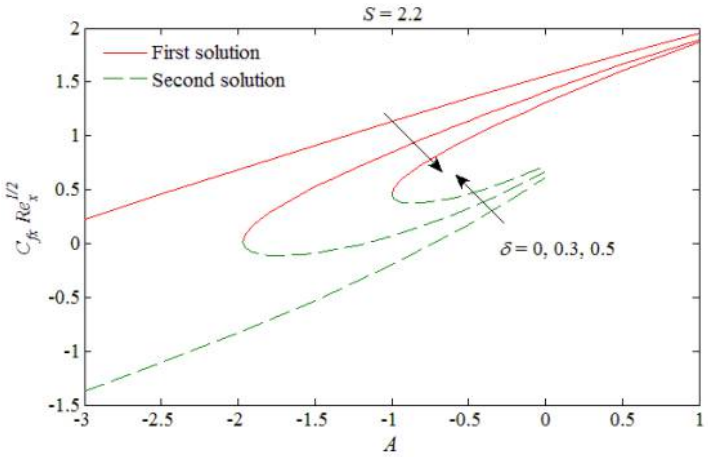

Figure 17: The skin friction $C_f \, \mathrm{Re}_x^{1/2}$ versus A for different values of δ .

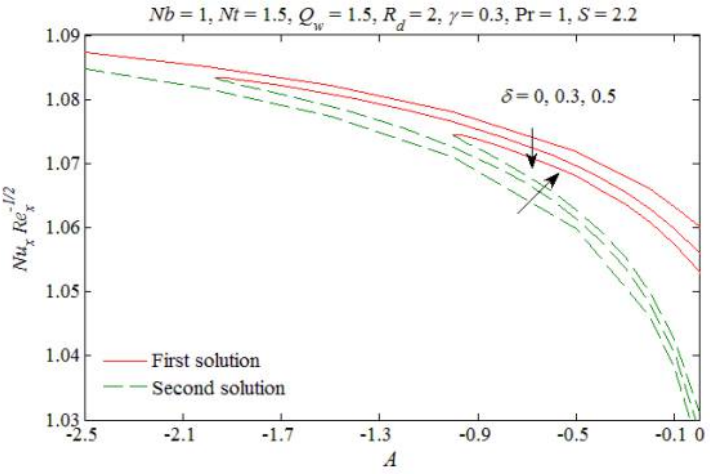

Figure 18: The Nusselt number $Nu_x \, \mathrm{Re}_x^{-1/2}$ versus A for different values of δ.

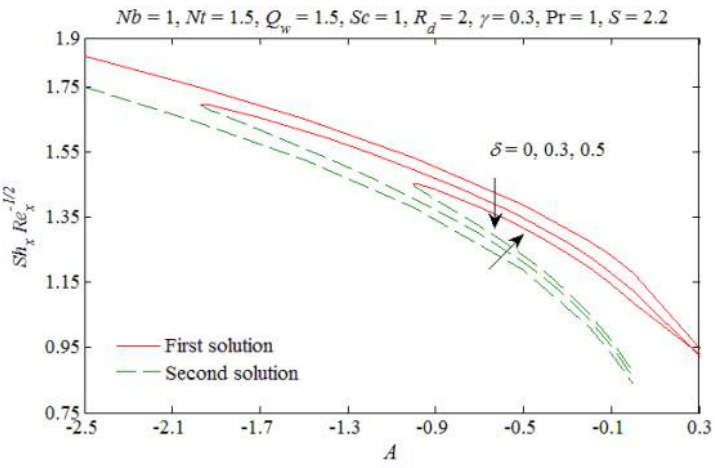

Figure 19: The Sherwood number $Sh_x \, \mathrm{Re}_x^{-1/2}$ versus A for different values of δ.

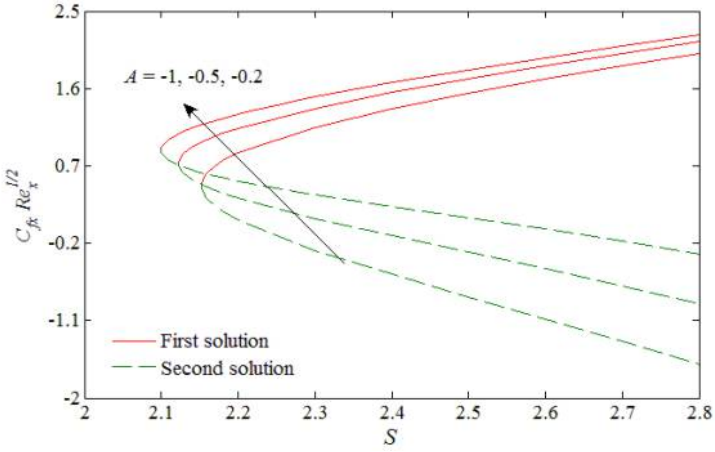

Figure 20: The skin friction $C_f \, \mathrm{Re}_x^{1/2}$ versus S for different values of A.

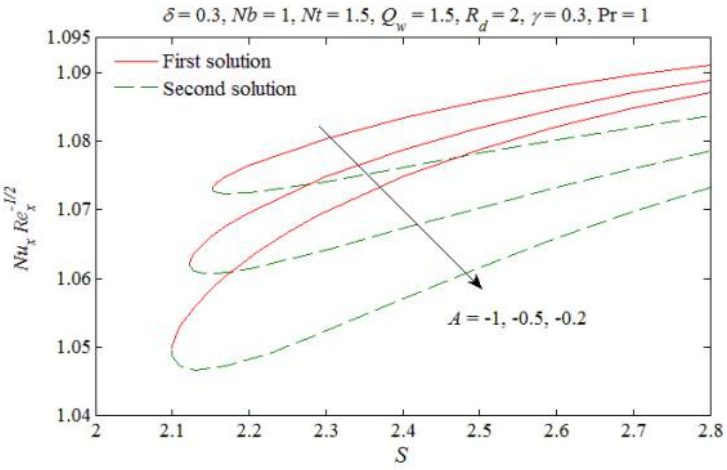

Figure 21: The Nusselt number $Nu_x \, \mathrm{Re}_x^{-1/2}$ versus S for different values of A.

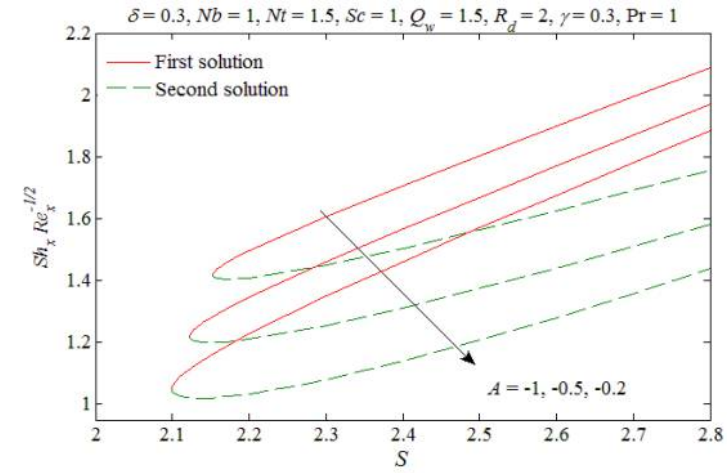

Figure 22: The Sherwood number $Sh_x \, \mathrm{Re}_x^{-1/2}$ versus S for different values of A.

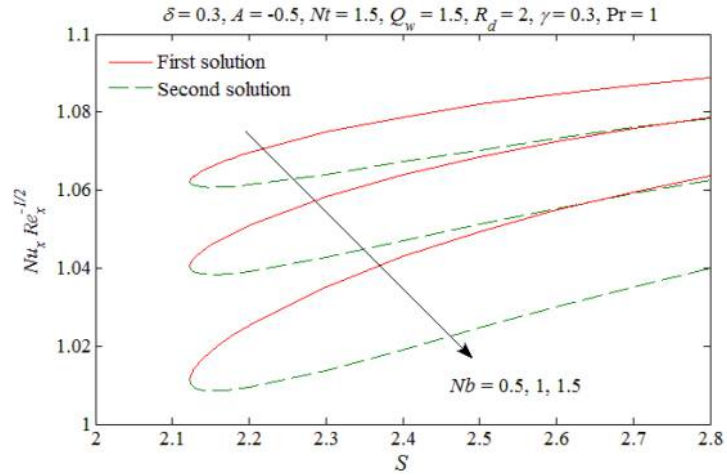

Figure 23: The Nusselt number $Nu_x \, \mathrm{Re}_x^{-1/2}$ versus S for different values of Nb.

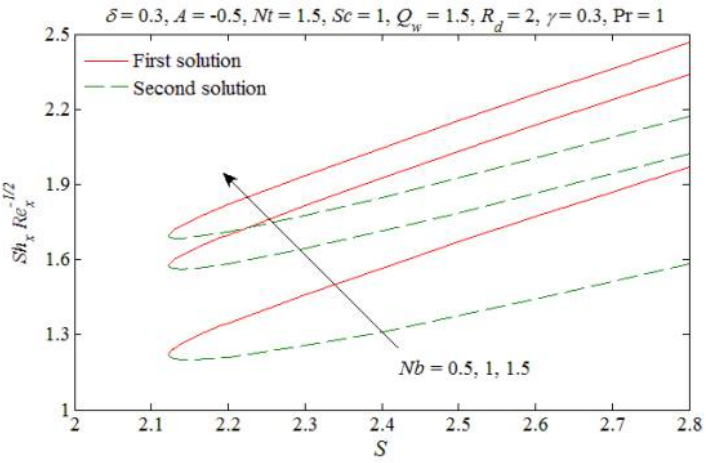

Figure 24: The Sherwood number $Sh_x \, \mathrm{Re}_x^{-1/2}$ versus S for different values of Nb.

Nomenclature

a, c, d positive constants

A unsteady parameter

A_1 first Rivilin-Erickson tensor

$\&$ concentration of nanoparticles

C_f skin friction coefficient

c_p specific heat

D_B Brownian diffusion

D_T coefficients of thermophoresis diffusion

f dimensionless stream function

h_f coefficient of heat transfer

I identity tensor

k thermal conductivity

$\&$ mean absorption coefficient

m_w mass flux

Nb Brownian motion parameter

Nt thermophoresis parameter

Nu_x local Nusselt number

Pr Prandtl number

q_r radiative heat flux

q_w heat flux

Re_x local Reynolds number

R_d radiation parameter

S Cauchy stress tensor

S suction parameter

Sc Schmidt number

t time

T temperature

T_f temperature of the hot fluid

T_∞ free stream temperature

T_w fluid wall temperature

v_w variable velocity of suction

v_0 positive constant

u, v velocity components

x, y Cartesian coordinates

Greek symbols

α thermal diffusivity

δ Williamson parameter

τ extra stress tensor

γ convective parameter

π second invariant tensor

θ dimensionless temperature

θ_w temperature ratio parameter

ν kinematic viscosity

μ_0 limiting viscosity at zero shear stress

μ_∞ limiting viscosity at infinite shear stress

$(\rho c_p)_f$ specific heat capacitance of nanofluid

σ ratio b/w the heat capacity and specific heat capacitance of nanoparticle

τ_w shear stress in $x-$ direction

σ^* Stefan-Boltzmann constant

ψ stream function

η similarity variable

Γ time constant

Subscripts

w condition at wall

∞ condition at free stream

Superscripts

$'$ derivative w.r.t. η